Experimental investigation of secondary flow in a heated channel using PIV and LIF simultaneously

Jaroslav Pulec[1*], *Václav* Vinš[2], and *Petra* Dančová[1]

[1]Technical University of Liberec, Faculty of Mechanical Engineering, Department of Power Engineering Equipment, Studentská 1402/2, 461 17 Liberec, Czech Republic
[2]Institute of Thermomechanics of the Czech Academy of Sciences, Dolejškova 1402/5, 182 00 Praha 8-Libeň, Czech Republic

Abstract. This paper describes an investigation of thermo-convective structures called Rayleigh-Bénard-Poiseuille (RBP) convection in a wide rectangular water channel formed above a heated bottom-wall. The phenomenon was investigated experimentally using planar Particle Image Velocimetry (PIV) for velocity vector field data and 2-color Laser-Induced Fluorescence (LIF) for temperature scalar field data. The PIV and LIF records were taken simultaneously on three cameras (one for PIV and two for LIF) in the central vertical plane of the channel in order to detect the secondary flow caused by the natural convection. The result is the combined temperature and velocity data used to evaluate the onset point of the secondary flow. The manifestation of this phenomenon on both velocity and temperature fields is described. The LIF method was confirmed to give more satisfactory results because the PIV method is generally less suitable for lower velocity measurement in boundary layers, both because of adverse reflections and because of the limitation for measuring very low velocities near walls. The measured data were compared with theoretical dependencies and with the literature data. Other limitations of the measurement were described, and steps for its improvement were suggested. In the present setup, temperature influence by the laser or wall accumulation was observed, which needs to be investigated more thoroughly and eliminated in future work.

1 Introduction

Thermoconvective structures in ducts with heated or cooled walls have been experimentally investigated for several decades. Rayleigh-Bénard-Poiseuille (RBP) flow is a specific case of convection in a parallel-plate horizontal channel with a heated bottom wall or cooled upper wall. It is mixed convection consisting of a primary forced flow and a secondary flow caused by heat transfer near the wall.

Many experimental studies on this phenomenon have been published since the 1980's. Osborne and Incropera [1] performed an investigation of the top and bottom-wall heating effect in a wide rectangular channel. Shortly afterward, Incropera et al. [2] published a paper dealing with a specific longitudinal roll. The work was specified in a paper by Maughan and Incropera [3]. Similar works can be mentioned in recent years, namely by Benderradji et al. [4], Mey et al. [5], and Taher and Abid [6]. An example of a numerical study by Rahli et al. [7] can also be given.

According to the previous papers, it can be said that the position of the onset point of the secondary flow moves downstream with decreasing heat flux density in the heated bottom-wall section and with increasing volumetric flow rate. Park et al. [8] performed a numerical study where, among other things, they determined the correlation dependence of the onset point of the secondary flow position on the heat flux density and flow rate, respectively, Rayleigh and Reynolds numbers. They calculated the correlation dependence

$$X_c = 56\mathrm{Ra}_q^{-\frac{3}{4}}, \text{for Pr} = 7, \quad (1)$$

where X_c is the dimensionless longitudinal distance to the onset point of intrinsic instability, which is related to the thermal stability of the system, which gradually leads to a developed turbulent flow, and Ra_q is the modified Rayleigh number for the input heat flux density q. This equation holds for Prandtl number Pr = 7, that is, for water under normal conditions. They also described that this distance value is a fraction of the distance to the point where there is a sharp increase in the heat transfer coefficient due to more intense cooling, i.e., the area of secondary flow formation. This is the region where the thickness of the temperature boundary layer increases rapidly, and the mixing of rising warmer water and falling cooler water begins to occur. Park et al. set the onset point of the secondary flow as $X_u = 4X_c$ or $6X_c$ depending on the amplitude of the velocity disturbances and determined that $X_u = 4X_c$ is valid for $\mathrm{Ra}_q < 3 \cdot 10^7$ and $X_u = 6X_c$ for $\mathrm{Ra}_q > 10^8$.

In connection with this research, preliminary measurements were made using the LIF method in a 1-color arrangement. For simplicity, Pulec et al. [9] investigated only the case of natural convection on the same experimental track. In this case, convective structures are not drifted by the forced flow, resulting in more significant temperature gradients that are more

* Corresponding author: jaroslav.pulec@tul.cz

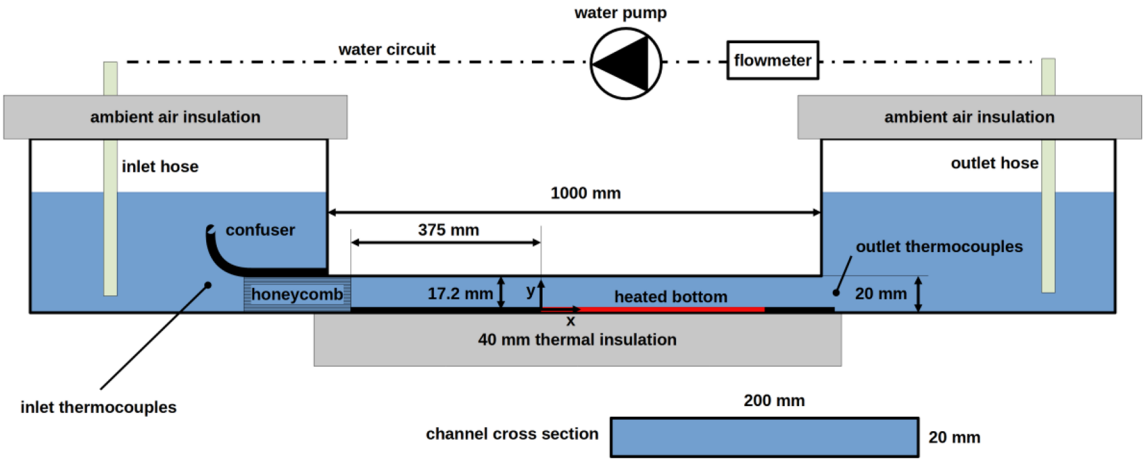

Fig. 1. Experimental setup.

easily detected by the method. Based on this work, the disadvantage of a 1-color arrangement was verified. Fluctuations in laser power cause sudden changes in illumination intensity to be misinterpreted as a change in temperature.

This work is an extension of previous studies, in particular, the use of modern experimental methods. In the past, both PIV and LIF have been used to study this phenomenon, but not simultaneously. This approach introduces many complications, especially with the different signal strength requirements of each method. Still, the benefit is the combined velocity and temperature data without the need to repeat measurements under very similar but not identical conditions.

The data obtained is the first successful experiment, and the know-how gained from this paper and from [9] will be used for more detailed research.

2 Methods

2.1 Particle Image Velocimetry

The optical method PIV was used for velocity vector field measurement, specifically the PIV system by LaVision Company, with all equipment for the 2D PIV recording . The specifications are as follows:

- 1 pcs sCMOS 5.5 MPx camera, resolution 2560 × 2160 pixels, 16 bit, exposure time 15 µs, spectral range 370 nm to 1100 nm, double-frame rate 15 Hz.
- Band-Pass filter 532 nm.
- Nd:YAG double-cavity laser, wavelength 532 nm, repetition frequency 15 Hz, pulse duration 10 nm, and pulse A energy 119 and 61.2 mJ pulse B energy.
- 10 µm hollow glass sphere particles.

2.2 Laser-Induced Fluorescence

LIF system uses the same apparatus as 2D PIV. There are two more sCMOS cameras with BP filters of 550 nm and 600 nm. The data was taken by DaVis 10.2 with an extension for LIF measurement in liquids. Both cameras were set to a single-frame mode for pulse A. Two fluorescent dyes were used: Rhodamine B as temperature dependent dye (LIF-T) and Rhodamine 110 as temperature independent dye (LIF-C).

3 Experimental setup

Fig. 1 illustrates the experimental setup. Two side glass tanks are connected by a 1000 mm long glass experimental channel with a cross-section of 200 × 20 mm. The channel inlet is realized by a confuser and honeycomb composed of small thin pipes. The heating of the bottom is realized by an inserted black painted aluminum sheet, which is equipped with a heating foil with dimensions of 200 × 384 mm. The height of the channel above the plate is 17.2 mm. The length for developing the laminar velocity profile is 375 mm. The experimental channel is insulated from below with 40 mm polystyrene. The channel is connected to a circulating pump with a flow meter via hoses. The water level is protected from the surrounding environment by insulation boards. The inlet and outlet are equipped with a set of thermocouples to measure the temperature conditions of the inlet and outlet flow.

The flow rate was regulated by the voltage applied to the pump using a DC power supply and controlled by a flow meter with a data acquisition unit. The power on the heating foil was regulated by a second channel on the same source. As Fig. 2 shows, there are three cameras; one for 2D PIV signal and two for LIF signal. Cameras take images of the illuminated plane by laser sheet along the horizontal centreline of the channel. The left side of the recorded plane is aligned with the beginning of the heated segment.

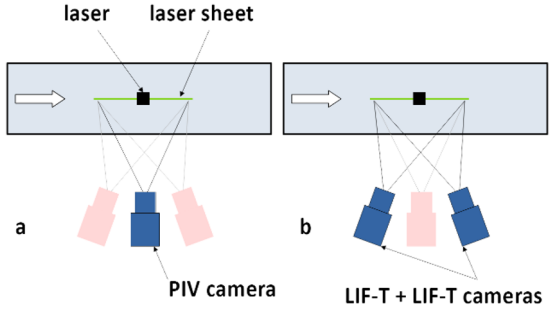

Fig. 2. Camera setup, top view. ***a*** PIV measurement setup, ***b*** LIF measurement setup.

4 Results and discussion

The PIV and LIF data were recorded simultaneously, and the velocity vector fields and scalar temperature fields for each mode were calculated from them. The modes are summarized in Table 1. The values correspond to the average during each data collection.

Table 1. Measured modes.

Mode	t_i (°C)	Q (l · s^{-1})	q (W · m^{-2})
0	24.33	1.22	0
1	24.28	1.15	65.12
2	24.17	1.2	129.56
3	24.13	1.22	258.82
4	24.13	1.27	385.92
5	23.95	1.22	516.49
6	23.90	1.26	645
7	23.40	1.23	779.24

4.1 Velocity maps

Fig. 3 shows averaged longitudinal scalar x-velocity fields for modes 0 – 7 in the vertical central plane. The flow goes from left to right, and the left edge of the map is at the beginning of the heated section. Zero-value on the position scale represents the center of PIV images and does not relate to the beginning of the heated area. Mode 0 was captured without heating, and there is a symmetrical velocity profile. The deformation of velocity profiles shifted upstream with rising heat flux density represents an effect of a secondary flow induced by natural convection.

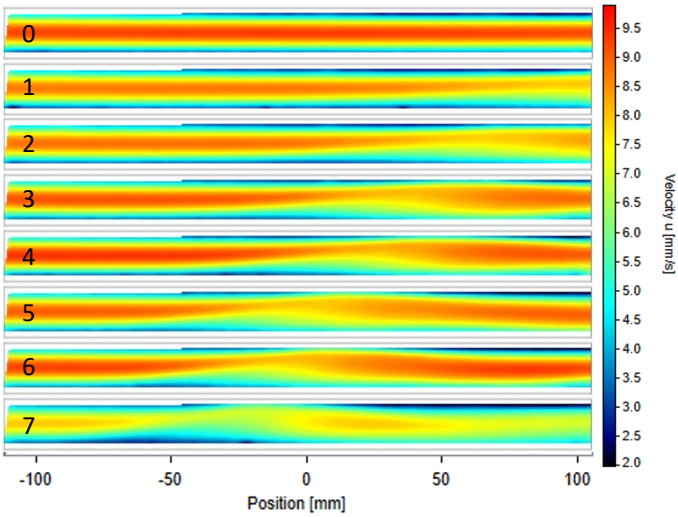

Fig. 3. Scalar fields: the x-velocity component for modes 0 – 7.

For the y-velocity component, see Fig. 4. The secondary flow is evident here with rising heat flux density. However, mode 0 also shows the non-zero vertical velocity on the right side of the map. It can be assumed that this is a consequence of the previous heating of the channel material or a consequence of the thermal effect of the laser. This may also affect the results in modes 1 – 7. y-velocity component reaches values up to 2.6 mm at the largest heat flux of 779 W · m^{-2}. s^{-1}

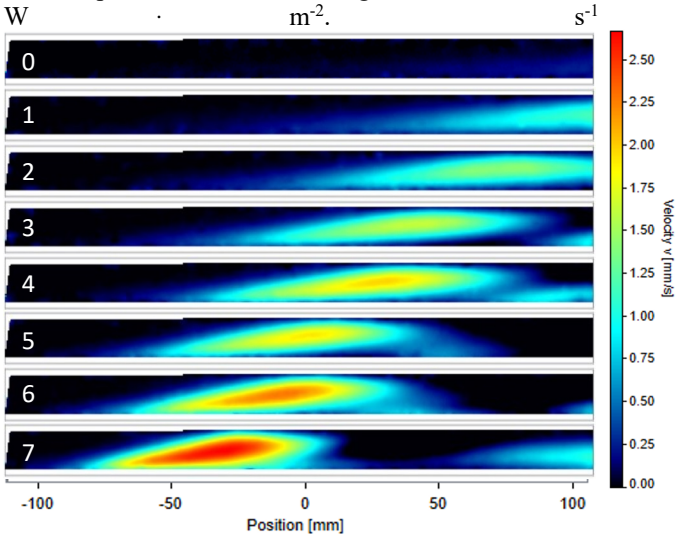

Fig. 4. Scalar fields: the y-velocity component for modes 0 – 7.

4.2 Temperature maps

Temperature fields are shown in Fig. 5. A rising strip of several degrees of Celsius warmer fluid is clearly visible. This view corresponds visually with, for example, visualization data of Incropera et al. [2] and Maughan and Incropera [3]. However, the results are affected by bubbles that settle at the top wall and obstruct the laser sheet. This effect is visible in these data as concentric lines across the viewing plane.

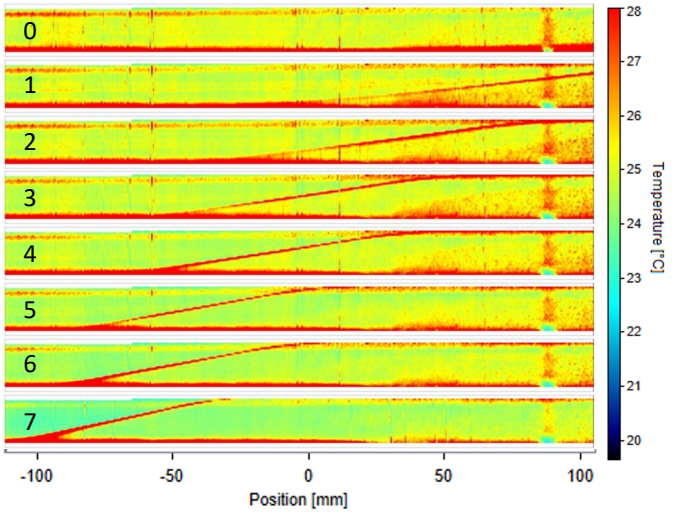

Fig. 5. Scalar fields: the temperature for modes 0 – 7.

4.3 Determination of the onset point of secondary flow

The results in Sections 4.1 and 4.2 show the same phenomenon represented by different variables. It can be said that PIV is not a very suitable method for measuring very low velocities in boundary layers, so it is difficult to assess the area where secondary flow is

occurring. In Fig. 6, see the waveform of temperature and *y*-velocity near the bottom for mode 7. A slight increase in velocity can be noticed, while the temperature waveform shows a sharp increase. From this, it can be said that LIF is more suitable than PIV for determining the onset point of the secondary flow in the current configuration. The *x*-position was determined from the left foot of the peak in every mode.

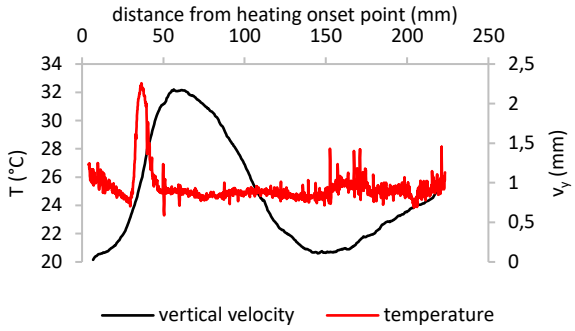

Fig. 6. *y*-velocity and temperature waveforms near the bottom for mode 7.

4.4 Results comparison

Fig. 7 shows experimental results in dimensionless quantities. The horizontal axis is longitudinal coordinate X. Vertical axis is modified Rayleigh number Ra_q. The dashed line is the onset distance of intrinsic instability X_u according to equation (1). The dash-dotted line is the onset distance of secondary flow X_u as $X_u = 4X_c$ for $Ra_q < 3 \cdot 10^7$ by Park [8]. Blue and green marks with dotted trend lines are from Benderradji's experiment [4] for Reynolds number Re = 50 and Re = 100, respectively. Although the shape of the curves X_c and X_u, according to Park, is independent of the Reynolds number because Re is included in the definition of the dimensionless coordinate, a rightward shift of the curves with increasing Re can be noticed in Benderradji's experimental data. The red marks are the current PIV-LIF data. The top five marks track well with Park's X_u dash-dotted trend and Benderradji's green trend. The value of X_c for the bottom two points is lower than can be predicted from the trends. This may be due to insufficiently stable thermal conditions or the thermal influence of the laser, as mentioned in chapter 4.1. Possible laser influence can also have a negative effect on the other points, but at lower values of the heat flux, this effect is more pronounced, so the points are significantly more to the left of the trends. Both possible causes need to be further investigated.

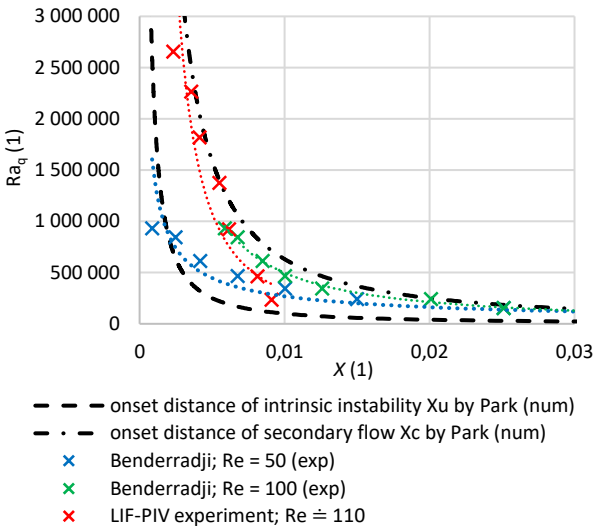

Fig. 7. Data comparison in dimensionless coordinates.

5 Conclusion

Mixed convection in the wide rectangular water channel was investigated using PIV and LIF methods simultaneously. Used methods and experimental setup were briefly described. The results were presented as scalar maps of temperature and velocity, and the onset point of secondary flow was compared in the graph with the results of other authors.

The presented data show good agreement with the results of other authors. However, there is a mismatch in the area of low heat fluxes. This may be the effect of the laser energy or additional heat flux from warm walls. This effect needs to be focused on in future work.

The results show that the experimental methods can be used to investigate the secondary flow phenomena. However, each method has its limits. PIV is problematic in the case of determining very low velocities, which do occur in the area with the onset of secondary flow. LIF is susceptible to changes in optical parameters during the experiment, for example, in the form of bubbles, but these are continuously expelled from the water during heating.

Future work will focus on measurements at different flow rates.

Nomenclature

symbol	unit	variable
g	$m \cdot s^{-2}$	gravitational acceleration constant
H	m	channel height
k	$W \cdot m^{-1} \cdot K^{-1}$	thermal conductivity of water
Pr	1	Prandtl number; ν/α
q	$W \cdot m^{-2}$	heat flux density
Q	$m^3 \cdot s^{-1}$	flow rate
Ra_q	1	modified Rayleigh number; $g\beta H^4 q/k\alpha\nu$
Re	1	Reynolds number; Hv_x/ν
t_i	°C	inlet temperature
v_x, v_y	$m \cdot s^{-1}$	x-, y-component of velocity
x, y	m	Cartesian coordinates
X	1	dimensionless coordinate; $x/\mathrm{PrRe}H$
X_c	1	dimensionless onset distance of intrinsic instability
X_u	1	dimensionless onset distance of secondary flow
greek symbols		
α	$m^2 \cdot s^{-1}$	thermal diffusivity
β	K^{-1}	volumetric thermal expansion coefficient
ν	$m^2 \cdot s^{-1}$	kinematic viscosity

This work was supported by the Student Grant Competition of the Technical University of Liberec under the project No. SGS-2022-5006.

References

1. Osborne and Incropera, "Laminar, mixed convection heat transfer for flow between horizontal parrallel plates with asymmetric heating," *J. Heat and Mass Transfer,* vol. 28, no. 1, pp. 207-219, 1985.
2. Incropera, Knox and Maughan, "Mixed-Convection Flow and Heat Transfer in the Entry Region of a Horizontal Rectangular Duct," *J. Heat Transfer,* vol. 109, no. 2, pp. 434-439, 1987.
3. Maughan and Incropera, "Secondary flow in horizontal channels heated from below. J. Experiments in Fluids," *J. Experiments in Fluids,* vol. 5, no. 5, pp. 334-343, 1987.
4. Benderradji, Haddan, Taher, Médale, Acid and Papini, "Characterization of fluid flow patterns and heat transfer in horizontal channel mixed convection," *J. Heat and Mass Transfer,* vol. 44, no. 12, pp. 1465-1476, 2008.
5. Mey, Westhoff and Wagner, "Experimental Investigation of Flow Structure Formation in a Heated Duct Flow," in *Dillmann A., Heller G., Kreplin HP., Nitsche W., Peltzer I.: New Results in Numerical and Experimental Fluid Mechanics VIII. Notes on Numerical Fluid Mechanics and Multidisciplinary Design*, Berlin, Springer, 2013.
6. Taher and Abid, "Experimental determination of heat transfer in a Poiseuille-Rayleigh-Bénard flow," *J. Heat and Mass Transfer,* no. 54, pp. 1453-1466, 2018.
7. O. Rahli, R. Bennacer, K. Bouhadef and D. E. Ameziani, "Numerical Heat Transfer, Part A: Applications: An International Journal of Computation and Methodology," *Numerical Heat Transfer,* no. 59, pp. 349-371, 2011.
8. J. H. Park, T. J. Chung, E. S. Yun, M. C. Kim and C. K. Choi, "The onset of longitudinal vortex rolls in the thermal entrance region of plane Poiseuille flow heated with a constant heat flux," *International Journal of Heat and Mass Transfer,* no. 49, pp. 3708-3716, 2006.
9. J. Pulec, P. Mony, V. Vinš and P. Dančová, "Preliminary measurements of the thermal field in a rectangular channel by the Planar Laser-Induced Fluorescence method," *EPJ Web of Conferences,* no. 264, 2022.